# Kim model for magnetization of type-II superconductors

D.-X. Chen[a] and R. B. Goldfarb
*Electromagnetic Technology Division, National Institute of Standards and Technology,*[b]
*Boulder, Colorado 80303*

(Received 31 January 1989; accepted for publication 18 May 1989)

We have calculated the initial magnetization curves and complete hysteresis loops for hard type-II superconductors. The critical-current density $J_c$ is assumed to be a function of the internal magnetic field $H_i$ according to Kim's model, $J_c(H_i) = k/(H_0 + |H_i|)$, where $k$ and $H_0$ are constants. As is the case for other critical-state models, additional assumptions are that bulk supercurrent densities are equal to $J_c$, and that the lower critical field is zero. Our analytic solution is for an infinite orthorhombic specimen with finite rectangular cross section, $2a \times 2b$ ($a \leqslant b$), in which a uniform field $H$ is applied parallel to the infinite axis. Assuming equal flux penetration from the sides, we reduced the two-dimensional problem to a one-dimensional calculation. The calculated curves are functions of $b/a$, a dimensionless parameter $p = (2ka)^{1/2}/H_0$, and the maximum applied field $H_m$. The field for full penetration is $H_p = H_0[(1+p^2)^{1/2} - 1]$. A related parameter is $H_m^* = H_0[(1+2p^2)^{1/2} - 1]$. Hysteresis loops were calculated for the different ranges of $H_m$: $H_m < H_p$, $H_p < H_m < H_m^*$, and $H_m^* < H_m$. The equations for an infinite cylindrical specimen of radius $a$ are the same as those for a specimen with square cross section, $a = b$. In the limit $p \ll 1$ and $a = b$, our results reduce to those of the Bean model ($J_c$ independent of $H_i$) for cylindrical geometry. Similarly, in the limit $p \ll 1$ and $b \to \infty$, the results are the same as those for a slab in the Bean model. For $H > 1.5\, H_p$, or $H > 0$ when $p \ll 1$, the width of the hysteresis loop $\Delta M$ may be used to deduce $J_c$ as a function of $H$: $J_c(H) = \Delta M(H)/[a(1 - a/3b)]$.

## I. INTRODUCTION

To derive magnetic properties of hard type-II superconductors, Bean[1,2] and London[3] introduced what has come to be known as the critical-state model.[4,5] The model assumes that penetrated supercurrents flow with a density equal to the critical-current density $J_c(H_i)$, where $H_i$ is the local internal field. The flux vortex array is stable and there is no flux creep. The lower critical field is zero. In Bean's model, $J_c(H_i)$ was considered to be a constant independent of $H_i$. Since then, several different $J_c(H_i)$ functions have been proposed. Kim, Hempstead, and Strnad[4,5] assumed that

$$J_c(H_i) = k/(H_0 + |H_i|)\,, \tag{1}$$

where $k$ and $H_0$ are positive constants (Kim's model). Watson[6] considered a simple linear function,

$$J_c(H_i) = A - C|H_i|\,, \tag{2}$$

where $A$ and $C$ are positive constants (linear model). Irie and Yamafuji[7] and Green and Hlawiczka[8] proposed a power-law model:

$$J_c(H_i) = k_1|H_i|^{-q}\,, \tag{3}$$

where $k_1$ and $q$ are positive constants. Fietz *et al.*[9] and Karasik, Vasil'ev, and Ershov[10] proposed an exponential-law model:

$$J_c(H_i) = A_1 \exp(-|H_i|/C_1)\,, \tag{4}$$

in which $A_1$ and $C_1$ are positive constants.

In principle, the initial magnetization curve and hysteresis loops of superconductors can be derived for every model mentioned above. Kim *et al.*[5] obtained two sections of the high-field loop for cylinders. Hulbert[11] solved for the initial curve and high-field loop for cylinders. Fietz *et al.*[9] derived the initial curve and high-field loop for an infinite slab using the Kim model and a nonzero lower critical field. Watson[6] derived the initial curve for a cylindrical sample and calculated the loop for low fields. Irie and Yamafuji[7] derived the high-field loop for a slab. Ohmer and Heinrich[12] and Wollan and Ohmer[13] derived the initial curve and the low-, medium-, and high-field loops for a cylinder, for $H_0 = 0$ in Kim's model, and $q = 1$ in the power-law model. Karasik *et al.*[10] and Ravi Kumar and Chaddah[14] gave analytic solutions for the initial curves for cylinder and slab samples, respectively, using the exponential-law model. The latter also gave numerical solutions for the hysteresis loops.

In this paper we use Kim's model to analytically derive both the initial magnetization curve and the hysteresis loops for an orthorhombic sample. The equations are somewhat complicated because there are two constants in the expression for $J_c(H_i)$ and the sample shape is not simple. The loops may be of three types, depending on the value of the maximum applied field. In addition, each curve has several stages.

One of the motivations for using Kim's model for the derivation is that, of the models listed above, this one is quite general. It subsumes the linear model when $H_0 \gg H_i$, and Bean's model when both $k$ and $H_0$ become infinite in such a way that $k/H_0$ is a constant. It becomes a power-law model for $q = 1$ if $H_0 = 0$. A practical motivation is that, by using Kim's model, we can more accurately predict the magnetic properties of superconductors for a realistic orthorhombic

[a] Permanent address: Department of Solid State Physics, Royal Institute of Technology, S100-44 Stockholm, Sweden.
[b] Formerly the National Bureau of Standards.

geometry. The physical significance of $H_0$ is discussed by Hulbert.[11]

The paper is organized as follows. Section II gives the general equation of magnetization for the orthorhombic geometry. Section III derives the magnetization as a function of field for different field ranges. Expressions are obtained for the initial curves and the hysteresis loops. Section IV uses the equations to generate hysteresis loops for several cases. In Sec. V, the formulas are simplified for a general orthorhombic Bean model. In Sec. VI, it is shown how $J_c(H)$ may be obtained from the width of the hysteresis loop.

## II. GENERAL EXPRESSIONS FOR MAGNETIZATION

### A. Orthorhombic geometry

We consider an infinitely long orthorhombic sample with cross section $2a\times 2b$ $(b\geqslant a)$. The boundaries of the sample are at $x=\pm a$ and $y=\pm b$. An external field $H$ is applied along the $z$ axis. The configuration of the sample and field direction are shown in Fig. 1(a). In this configuration, the magnetic quantities have only $z$ components, and the supercurrents have only $x$ and $y$ components.

The critical-state model involves only macroscopic supercurrent, magnetization, flux density, and field. The lower critical field is assumed to be zero. The local internal field $H_i$ is defined as

$$H_i = B/\mu_0 , \tag{5}$$

where $B$ is the macroscopic local flux density and $\mu_0$ is permeability of free space. If $H$ is the applied field and $M_i$ is the local magnetization, that is, the field produced by bulk supercurrents, we have

$$M_i = H_i - H . \tag{6}$$

The total magnetization $M$ is the average of $M_i$ over the sample cross section.

Solutions for an infinitely wide slab or an infinitely long cylinder involve only one variable of integration. We have to consider a two-dimensional problem for an orthorhombic sample. Fortunately, this two-dimensional problem can be simplified to a one-dimensional calculation. Because the sample is infinitely long and is located in a uniform $H$, both $H_i$ and $J_c(H_i)$ along the sample surface must be the same on each side. Furthermore, the supercurrents penetrate the same depth into the sample from each side. The supercurrent path is the rectangular circuit shown in Fig. 1(a). For an infinitely long sample, the supercurrent density $J$, $H_i$ and $M_i$ along a given circuit are uniform and are written as functions of $x$: $J(x)$, $H_i(x)$, and $M_i(x)$.

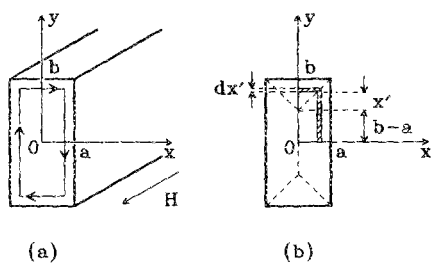


(a) (b)

FIG. 1. (a) Sample configuration. (b) Supercurrent path.

To obtain the total magnetization $M$, we have to integrate $M_i(x)$ over the cross-sectional area. Because $M$ is an average over the sample and because of symmetry, it is sufficient to take only the first quadrant $(x>0,\ y>0)$ into consideration. In this case the area is $ab$, and the differential area element is $(2x'+b-a)dx'$, as shown in Fig. 1(b). Thus,

$$M = \frac{1}{ab}\int_0^a (2x'+b-a)M_i(x')\,dx' . \tag{7}$$

In this equation we use primes to denote the variable of integration. In the remainder of the paper, the primes are omitted in the integrations.

### B. Extension to cylinders and other geometries

In the limit $b/a=1$, Eq. (7) for the average magnetization applies to a specimen with square cross section:

$$M = \frac{2}{a^2}\int_0^a xM_i(x)\,dx . \tag{7a}$$

The same expression applies to an infinite cylindrical specimen of radius $a$, where the area is $\pi a^2$ and the differential area element is $2\pi x\,dx$. Consequently, when $b$ is set equal to $a$, the $M(H)$ curves derived below are for either square specimens, with cross section $2a\times 2a$, or cylindrical specimens, with radius $a$.[15]

The principle of equal supercurrent penetration from each side allows us to extend these arguments to samples with cross sections in the shape of triangles and polygons. The only requirement is that all sides are tangent to a circle of radius $a$. A technologically useful example is a regular hexagon.

## III. DERIVATION OF $M(H)$ FROM $J(x)$

### A. General expression for $J(x)$

To obtain $M$ we have to first derive the supercurrent density $J(x)$. Using Ampere's law and Eq. (1), we have

$$\frac{dH_i}{dx} = -\operatorname{sgn}(J)J_c(H_i) = \frac{-\operatorname{sgn}(J)k}{H_0+\operatorname{sgn}(H_i)H_i} , \tag{8}$$

where sgn is the sign function, equal to $\pm 1$. From Eq. (8),

$$\int [H_0+\operatorname{sgn}(H_i)H_i]\,dH_i = -\int \operatorname{sgn}(J)k\,dx . \tag{9}$$

After integration, the solution for the quadratic in $H_i$, in a region where $H_i$ and $J$ do not change their signs, is

$$H_i = -\operatorname{sgn}(H_i)H_0 \pm [H_0^2 - \operatorname{sgn}(JH_i)2k(x+c)]^{1/2} , \tag{10}$$

where $c$ is an integration constant to be determined by the boundary conditions. Multiplying Eq. (10) by $\operatorname{sgn}(H_i)$, we obtain

$$H_0+\operatorname{sgn}(H_i)H_i = \pm\operatorname{sgn}(H_i)[H_0^2 - \operatorname{sgn}(JH_i)2k(x+c)]^{1/2} . \tag{11}$$

We set $\pm \operatorname{sgn}(H_i) = 1$ on the right-hand side because, from Eq. (1), the left-hand side is always positive. Using Eqs. (1) and (11) we obtain

$$J(x) = \operatorname{sgn}(J) J_c(H_i) = \operatorname{sgn}(J) k / [H_0 + \operatorname{sgn}(H_i) H_i]$$
$$= \operatorname{sgn}(J) k / [H_0^2 - \operatorname{sgn}(J H_i) 2k(x+c)]^{1/2} . \quad (12)$$

This is the general expression for $J(x)$.

### B. Initial $M(H)$ curve and full-penetration field

#### 1. Current densities and local fields

We start from the initial state, $H = M = 0$, and increase $H$ in the $z$ direction. According to Lenz's law, the supercurrent $J$ (of negative sign) will penetrate from the surface ($x = a$) inward. If the supercurrent penetrates until $x = x_0$, $H_i$ in the sample will be $H$ at $x = a$, decrease to 0 at $x = x_0$, and remain 0 for $x < x_0$. Figures 2(a) and 2(b) show the $J(x)$ and $H_i(x)$ functions, represented schematically by straight-line segments. If $H$ increases further, $x_0$ decreases. When $x_0 = 0$, the sample is completely penetrated [Figs. 2(c) and 2(d)]. The corresponding field is called the full-penetration field $H_p$. In the complete penetration state, $J(x)$ and $H_i(x)$ have similar forms, shown in Figs. 2(e) and 2(f).

For the initial magnetization curve, where the field is first applied to the sample, we will denote $J(x)$ as $J_0(x)$. We derive the supercurrent density $J_0(x)$ for $x_0 < x < a$. The boundary condition is

$$J_0(a) = -J_c(H) . \quad (13)$$

Substituting Eqs. (1) and (12) into Eq. (13), we have

$$[H_0^2 + 2k(a+c)]^{1/2} = H_0 + H , \quad (14)$$

from which

$$2kc = (H_0 + H)^2 - H_0^2 - 2ka . \quad (15)$$

Substituting Eq. (15) into Eq. (12), we obtain

$$J_0(x) = -k / [(H_0 + H)^2 - 2k(a-x)]^{1/2} \quad (x_0 < x < a) . \quad (16)$$

We consider the magnetization for two stages: $0 < H < H_p$ (stage I) and $H_p < H$ (stage II).

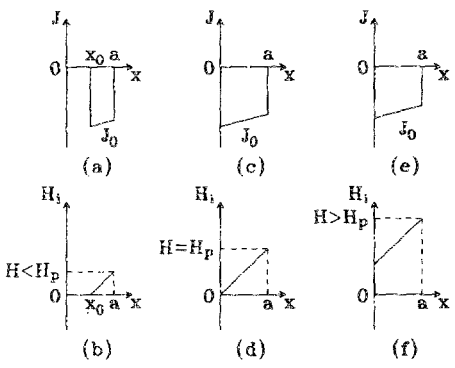


FIG. 2. Schematic supercurrent density $J$ and local internal field $H_i$ as functions of $x$ for the initial magnetizing process. For purposes of illustration, $J$ and $H_i$ are sketched as straight line segments.

#### 2. Stage I ($0 < H < H_p$)

In this range, $x_0$ decreases from $a$ to 0, and

$$H_i(x) = 0 \quad (0 < x < x_0) , \quad (17a)$$

$$H_i(x) = H + \int_x^a J_0(x)\, dx \quad (x_0 < x < a) . \quad (17b)$$

From Eqs. (17a), (17b), and (6) we obtain

$$M_i(x) = -H \quad (0 < x < x_0) , \quad (18a)$$

$$M_i(x) = \int_x^a J_0(x)\, dx \quad (x_0 < x < a) . \quad (18b)$$

From Eqs. (17b) and (16), $x_0$ is determined:

$$x_0 = a - [(H_0 + H)^2 - H_0^2]/2k , \quad (19)$$

using the boundary condition

$$H_i(x_0) = 0 . \quad (20)$$

Substituting Eqs. (18a), (18b), and (16) into Eq. (7), and using Eq. (19), we obtain the final result:

$$M(H) = -Hx_0(b - a + x_0)/ab$$
$$- S_1(b + x_0)(a - x_0)/ab$$
$$+ (S_1^3 - H_0^3)Q_1 + 2H_0^3(a - x_0)/5kab$$
$$(0 < H < H_p) , \quad (21)$$

where

$$S_1 = H_0 + H , \quad (22a)$$

$$Q_1 = [5k(a+b) - 2S_1^2]/15abk^2 . \quad (22b)$$

For the case $a = b$, applicable to cylinders of radius $a$, Eq. (21) reduces to Hulbert's Eq. (10d), with appropriate symbol substitutions of $H$ for $B$.[11] In the limit $b \to \infty$, for infinite slabs of thickness $2a$, Eq. (21) reduces to the solution of Fietz *et al.*, Eq. (b) in Table I of Ref. 9.

#### 3. Full-penetration field $H_p$

When $x_0$ in Eq. (19) becomes 0, the sample is completely penetrated [Figs. 2(c) and 2(d)]. Setting $x_0 = 0$ so that, by definition, $H = H_p$ in Eq. (19), we obtain

$$H_p = (H_0^2 + 2ka)^{1/2} - H_0 . \quad (23)$$

#### 4. Stage II ($H_p < H$)

In this range [Figs. 2(e) and 2(f)], Eqs. (7), (16), (17b), and (18b) are still valid with $x_0$ replaced by 0. The final result is

$$M(H) = -S_1 + (S_1^3 - R_1^3)Q_1 + 2R_1^3/5kb$$
$$(H_p < H < H_m) , \quad (24)$$

where

$$R_1 = (S_1^2 - 2ka)^{1/2} . \quad (25)$$

### C. Hysteresis loops for the low-$H_m$ case ($H_m < H_p$)

To obtain hysteresis loops we have to derive reverse $M(H)$ curves from a given maximum field $H_m$ on the initial curve. The reverse $M(H)$ curve starts from $(H_m, M_m)$ and ends at $(-H_m, -M_m)$, forming the descending branch of the hysteresis loop. The ascending branch will then be

$-M(-H)$. The equations governing the shape of the hysteresis loops depend on $H_m$. The first case is for $H_m < H_p$, where the specimen is never fully penetrated. The second case is for $H_m^* < H_m$, when the reverse supercurrent penetrates to the center of the specimen before $H$ is cycled back to zero. (The expression for $H_m^*$ is derived in Sec. III D 2.) The third case is intermediate, $H_p < H_m < H_m^*$.

### 1. Current densities and local fields

The low-$H_m$ reverse $M(H)$ curve starts from a point on stage I of the initial curve, $H_m < H_p$. Figures 3(a)–3(j) show the $J(x)$ and $H_i(x)$ functions developing with decreasing $H$. Figures 3(a) and 3(b), similar to Figs. 2(a) and 2(b), correspond to the starting point with $H = H_m$ and a negative supercurrent penetrating to $x_m$. When $H$ decreases from $H_m$, the induced supercurrent with positive $J$ will penetrate from the sample surface to $x = x_1$, and the corresponding $J(x)$ and $H_i(x)$ are shown in Figs. 3(c) and 3(d). At this point, $J(x)$ for $x_m < x < x_1$ [denoted as $J_m(x)$] remains the same as the $J_0(x)$ for the initial magnetization when $H = H_m$. $J(x)$ is $J_1(x)$ for $x_1 < x < a$. This arrangement is maintained until $H = 0$, as shown in Fig. 3(e) and 3(f). Further decreasing $H$ to a negative value complicates the situation. As shown in Figs. 3(g) and 3(h), the expression for $J(x)$ has to be divided into three parts: $J_m(x)$, $J_2(x)$, and $J_3(x)$, and the corresponding $H_i$ changes sign at $x = x_3$. This situation lasts until $H = -H_m$, when both $J_m$ and $J_2$ are removed. Figures 3(i) and 3(j) show $J(x)$ and $H_i(x)$ for $H = -H_m$; they are opposite to the case shown in Figs. 3(a) and 3(b).

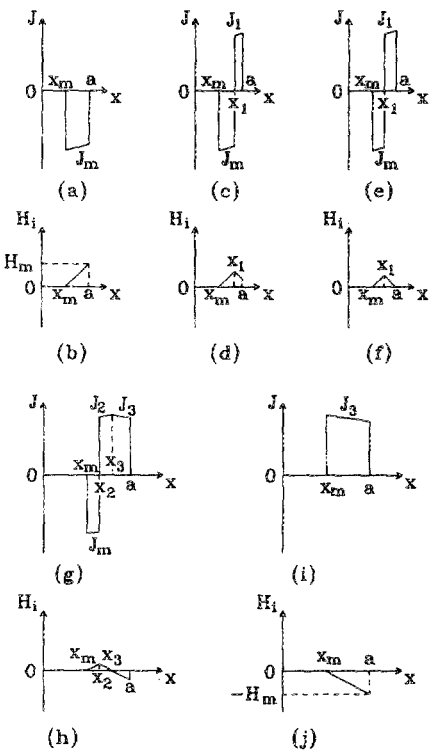


FIG. 3. Schematic supercurrent density and local internal field as functions of $x$ for the reverse magnetizing process from $H_m < H_p$.

We give the expressions for $J_m(x)$, $J_1(x)$, $J_2(x)$, and $J_3(x)$. Because $J_m(x) = J_0(x)$ when $H = H_m$, we obtain from Eq. (16):

$$J_m(x) = -k/[(H_0 + H_m)^2 - 2k(a-x)]^{1/2} \quad (x_m < x < x_1) . \tag{26}$$

The boundary condition for $J_1(x)$ is

$$J_1(a) = J_c(H) . \tag{27}$$

Substituting Eqs. (1) and (12) into Eq. (27) we have

$$[H_0^2 - 2k(a+c)]^{1/2} = H_0 + H , \tag{28}$$

from which

$$2kc = -(H_0 + H)^2 + H_0^2 - 2ka . \tag{29}$$

Substituting Eq. (29) into Eq. (11) we obtain

$$J_1(x) = k/[(H_0 + H)^2 + 2k(a-x)]^{1/2} \quad (x_1 < x < a) . \tag{30}$$

The boundary conditions for $J_2(x)$ and $J_3(x)$ are

$$J_2(x_3) = J_c(0) \tag{31a}$$

and

$$J_3(a) = J_c(H) . \tag{31b}$$

By a similar derivation, we obtain

$$J_2(x) = k/[H_0^2 + 2k(x_3 - x)]^{1/2} \quad (x_2 < x < x_3) \tag{32a}$$

and

$$J_3(x) = k/[(H_0 - H)^2 - 2k(a-x)]^{1/2} \quad (x_3 < x < a) . \tag{32b}$$

The magnetization process can be divided into two stages. Stage I corresponds to $0 < H < H_m$, and stage II corresponds to $-H_m < H < 0$.

### 2. Stage I ($0 < H < H_m$)

In stage I, $H_i(x)$ is

$$H_i(x) = 0 \quad (0 < x < x_m) , \tag{33a}$$

$$H_i(x) = H_m + \int_x^a J_m(x)\,dx \quad (x_m < x < x_1) , \tag{33b}$$

$$H_i(x) = H + \int_x^a J_1(x)\,dx \quad (x_1 < x < a) . \tag{33c}$$

From Eqs. (33a), (33b), and (33c) and Eq. (6), $M_i(x)$ is obtained as

$$M_i(x) = -H \quad (0 < x < x_m) , \tag{34a}$$

$$M_i(x) = H_m - H + \int_x^a J_m(x)dx \quad (x_m < x < x_1) , \tag{34b}$$

$$M_i(x) = \int_x^a J_1(x)\,dx \quad (x_1 < x < a) . \tag{34c}$$

$x_m$ can be determined by replacing $H$ in Eq. (19) with $H_m$:

$$x_m = a - [(H_0 + H_m)^2 - H_0^2]/2k . \tag{35a}$$

Using the continuity of $H_i$ at $x = x_1$, and from Eqs. (33b) and (33c), we obtain

$$x_1 = a - [(H_0 + H_m)^2 - (H_0 + H)^2]/4k . \quad (35b)$$

Substituting Eqs. (34a), (34b), (34c), (26), and (30) into Eq. (7), and using $x_m$ and $x_1$ defined by Eqs. (35a) and (35b) we obtain the final result:

$$\begin{aligned} M(H) = & -Hx_m(b-a+x_m)/ab \\ & - S_1[ab + (a-b)x_m - x_m^2]/ab \\ & - (S_1^3 - R_2^3)Q_2 + (R_2^3 - H_0^3)Q_3 \\ & + 2[(x_1 - a)R_2^3 + (x_1 - x_m)H_0^3]/5kab \\ & (0 < H < H_m) , \end{aligned} \quad (36)$$

where

$$S_2 = H_0 + H_m , \quad (37a)$$

$$R_2 = [S_1^2 + 2k(a - x_1)]^{1/2} , \quad (37b)$$

$$Q_2 = [5k(a+b) + 2S_1^2]/15abk^2 , \quad (37c)$$

$$Q_3 = [10k(a+b) + 3S_1^2 - 7S_2^2]/30abk^2 . \quad (37d)$$

### 3. Stage II ($-H_m < H < 0$)

In stage II, $H_i(x)$ and $M_i(x)$ are

$$H_i(x) = 0 \quad (0 < x < x_m) , \quad (38a)$$

$$H_i(x) = H_m + \int_x^a J_m(x)\,dx \quad (x_m < x < x_2) , \quad (38b)$$

$$H_i(x) = H + \int_x^{x_1} J_2(x)dx + \int_{x_1}^a J_3(x)dx \quad (x_2 < x < x_3) , \quad (38c)$$

$$H_i(x) = H + \int_x^a J_3(x)dx \quad (x_3 < x < a) , \quad (38d)$$

and

$$M_i(x) = -H \quad (0 < x < x_m) , \quad (39a)$$

$$M_i(x) = H_m - H + \int_x^a J_m(x)dx \quad (x_m < x < x_2) , \quad (39b)$$

$$M_i(x) = \int_x^{x_1} J_2(x)dx + \int_{x_1}^a J_3(x)dx \quad (x_2 < x < x_3) , \quad (39c)$$

$$M_i(x) = \int_x^a J_3(x)dx \quad (x_3 < x < a) . \quad (39d)$$

$x_m$ is given in Eq. (35a), and $x_3$ and $x_2$ can be derived using the continuity conditions at $x = x_3$ and $x_2$ from Eqs. (38d), (38c), and (38b):

$$x_3 = a - [(H_0 - H)^2 - H_0^2]/2k , \quad (40a)$$

$$x_2 = a - [(H_0 - H)^2 + (H_0 + H_m)^2 - 2H_0^2]/4k . \quad (40b)$$

The final result is obtained in the standard way used above:

$$\begin{aligned} M(H) = & \\ & -Hx_m(b-a+x_m)/ab + S_3(a-x_3)(b+x_3)/ab \\ & - S_1(x_3 - x_2)[2(b-a+x_2) + x_3 + x_m]/ab \\ & - (S_3^3 - H_0^3)Q_4 + (R_3^3 - H_0^3)(Q_5 + Q_6) \\ & + 2[(x_3 - a)H_0^3 - (x_3 - x_2)(R_3^3 - H_0^3)]/5kab \\ & (-H_m < H < 0) , \end{aligned} \quad (41)$$

where

$$S_3 = H_0 - H , \quad (42a)$$

$$R_3 = [H_0^2 + 2k(x_3 - x_2)]^{1/2} , \quad (42b)$$

$$Q_4 = [5k(a+b) - 2S_3^2]/15abk^2 , \quad (42c)$$

$$Q_5 = [5k(a+b) - 5S_3^2 + 7H_0^2]/15abk^2 , \quad (42d)$$

$$Q_6 = [10k(a+b) - 3S_3^2 - 7S_2^2 + 6H_0^2]/30abk^2 . \quad (42e)$$

## D. Hysteresis loops for the high-$H_m$ case ($H_m^* < H_m$)

### 1. Current densities and local fields

For $H_m > H_p$ we have to consider two cases. In the high-$H_m$ case, the reverse supercurrent completely penetrates to the sample center before $H$ has decreased to 0. This corresponds to $H_m > H_m^* = (H_0^2 + 4ka)^{1/2} - H_0$ as shown below. The second case is for medium $H_m$, where the reverse supercurrent is not completely penetrated when $H = 0$. This will be discussed in Sec. III E.

$J(x)$ and $H_i(x)$ for the high-$H_m$ case are shown in Figs. 4(a)–4(n). Figures 4(a) and 4(b) correspond to the starting point when $H = H_m$ and the sample is completely penetrated by negative supercurrent with density $J_m(x)$. Decreasing $H$ from $H_m$ induces a positive supercurrent with density $J_1(x)$. As can be seen in Figs. 4(c) and 4(d), the reverse positive supercurrent penetrates to $x = x_1$, at which point $H = H_{prh}$, the full reverse penetration field for the high-$H_m$ case, defined below. This is stage I.

Stage II starts when $x_1$ becomes 0, shown in Figs. 4(e) and 4(f), and ends when $H$ reaches 0, shown in Figs. 4(g) and 4(h). After that comes stage III, in which the local internal fields at the center and the surface of the sample have different signs, corresponding to different functions for $J_2(x)$ and $J_3(x)$, bounded by $x = x_3$, where $H_i = 0$. This situation is shown in Figs. 4(i) and 4(j). Further decreasing $H$ results in the situation of Figs. 4(k) and 4(l), when the whole sample has negative $H_i$, and the magnetization process enters stage IV. In stage IV, $J(x)$ keeps the form of $J_3(x)$ until $H = -H_m$, when the process ends. The final $J(x)$ and $H_i(x)$ are shown in Figs. 4(m) and 4(n).

The expressions for $J_m(x)$, $J_1(x)$, $J_2(x)$, and $J_3(x)$ have already been given in Eqs. (26), (30), (32a), and (32b), and we need only change the regions of $x$, referring to the figures as described above.

### 2. Stage I ($H_{prh} < H < H_m$)

In stage I, $H_i(x)$ and $M_i(x)$ are

$$H_i(x) = H_m + \int_x^a J_m(x)dx \quad (0 < x < x_1) , \quad (43a)$$

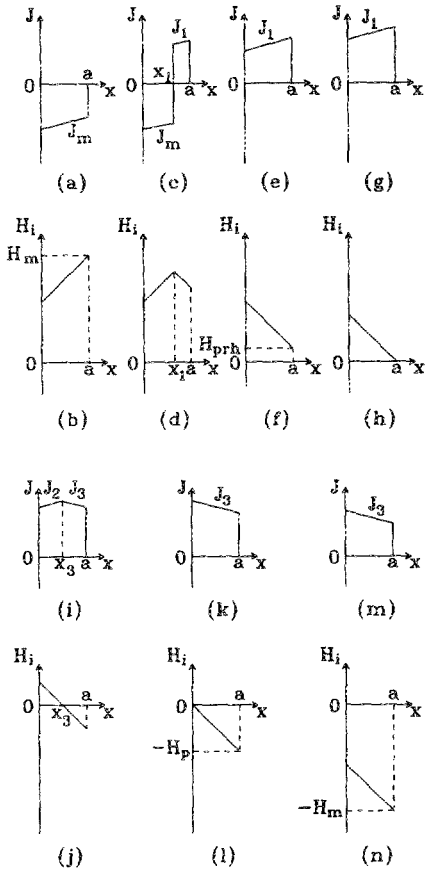


FIG. 4. Same as Fig. 3, from $H_m > H_m^*$.

$$H_i(x) = H + \int_x^a J_1(x)dx \quad (x_1 < x < a)\,, \tag{43b}$$

and

$$M_i(x) = H_m - H + \int_x^a J_m(x)dx \quad (0 < x < x_1)\,, \tag{44a}$$

$$M_i(x) = \int_x^a J_1(x)dx \quad (x_1 < x < a)\,. \tag{44b}$$

$x_1$ is given in Eq. (35b), and the final result is

$$M(H) = -S_1 - (S_1^3 - R_2^3)Q_2 + (R_2^3 - R_4^3)Q_3 + 2[(x_1 - a)R_2^3 + x_1 R_4^3]/5kab \quad (H_{prh} < H < H_m)\,, \tag{45}$$

in which

$$R_4 = (S_2^2 - 2ka)^{1/2}\,, \tag{46}$$

and $H_{prh}$ is the reverse full-penetration field for the high-$H_m$ case. It can be determined by taking $x_1 = 0$ in Eq. (35b):

$$H_{prh} = [(H_0 + H_m)^2 - 4ka]^{1/2} - H_0\,. \tag{47}$$

The boundary between the high- and medium-$H_m$ case can also be determined from Eq. (35b) by taking $x_1 = 0$ and $H = 0$:

$$H_m^* = (H_0^2 + 4ka)^{1/2} - H_0\,. \tag{48}$$

In the limit $b \to \infty$, Eq. (45) reduces to Eq. (d) in Table I, Ref. 9, with the typographic correction "...$\{(\sqrt{2}/2)[\ldots + 2B_0^2]^{3/2}\ldots\}$."

### 3. Stage II ($0 < H < H_{prh}$)

In stage II, the $H_i(x)$ and $M_i(x)$ are

$$H_i(x) = H + \int_x^a J_1(x)dx \quad (0 < x < a)\,, \tag{49}$$

$$M_i(x) = \int_x^a J_1(x)dx \quad (0 < x < a)\,. \tag{50}$$

$x_1$ is given in Eq. (35b), and the final result is

$$M(H) = -S_1 - (S_1^3 - R_5^3)Q_2 - 2R_5^3/5kb \quad (0 < H < H_{prh})\,, \tag{51}$$

where

$$R_5 = (S_1^2 + 2ka)^{1/2}\,. \tag{52}$$

For the case $a = b$, applicable to cylinders of radius $a$, Eq. (51) reduces to Kim's solution for $M(H)$ in the first quadrant, Eq. (14) in Ref. 5, and to Hulbert's solution, Eq. (10b) in Ref. 11. In the limit $b \to \infty$, for infinite slabs of thickness $2a$, Eq. (51) reduces to the solution of Fietz *et al.*, Eq. (e) in Table I of Ref. 9.

### 4. Stage III ($-H_p < H < 0$)

In stage III, the $H_i(x)$ and $M_i(x)$ are

$$H_i(x) = H + \int_x^{x_3} J_2(x)dx + \int_{x_3}^a J_3(x)dx \quad (0 < x < x_3)\,, \tag{53a}$$

$$H_i(x) = H + \int_x^a J_3(x)dx \quad (x_3 < x < a)\,, \tag{53b}$$

and

$$M_i(x) = \int_x^{x_3} J_2(x)dx + \int_{x_3}^a J_3(x)dx \quad (0 < x < x_3)\,, \tag{54a}$$

$$M_i(x) = \int_x^a J_3(x)dx \quad (x_3 < x < a)\,. \tag{54b}$$

$x_3$ is given in Eq. (40a), and the final result is

$$M(H) = S_3(a - x_3)(b + x_3)/ab - S_1 x_3(b - a + x_3)/ab - (S_3^3 - H_0^3)Q_4 - (H_0^3 - R_6^3)Q_5 - 2[(a - x_3)H_0^3 + x_3 R_6^3]/5kab \quad (-H_p < H < 0)\,, \tag{55}$$

where

$$R_6 = (H_0^2 + 2kx_3)^{1/2}\,. \tag{56}$$

The lower $H$ boundary in this stage is $-H_p$, as can be seen by taking $x_3 = 0$ in Eq. (40a). For the case $a = b$, applicable to cylinders of radius $a$, Eq. (55) reduces to Hulbert's Eq. (10c), with appropriate symbol substitutions of $H$ for $B$.[11] In the limit $b \to \infty$, Eq. (55) reduces to Eq. (g) in Table I, Ref. 9, with the typographic correction

"$-(\mathbf{B_0}+\mathbf{H_a}) + \ldots\{[\ldots - (B_0 - H_0)^2 + \ldots]^{3/2} - \ldots\} + \ldots$."

### 5. Stage IV ($-H_m < H < -H_p$)

In stage IV, the $H_i(x)$ and $M_i(x)$ are

$$H_i(x) = H + \int_x^a J_3(x)dx \quad (0 < x < a)\,, \tag{57}$$

$$M_i(x) = \int_x^a J_3(x)dx \quad (0 < x < a)\,, \tag{58}$$

and the final result is

$$M(H) = S_3 - (S_3^3 - R_7^3)Q_4 - 2R_7^3/5kb \quad (-H_m < H < -H_p)\,, \tag{59}$$

where

$$R_7 = (S_3^2 - 2ka)^{1/2}\,. \tag{60}$$

To generate the complete hysteresis loop, stages I–IV are reflected about the origin onto the third and fourth quadrants, as indicated at the beginning of Sec. III C. For example, Eq. (59) in the second quadrant becomes

$$M(H) = -S_1 + (S_1^3 - R_1^3)Q_1 + 2R_1^3/5kb \quad (H_p < H < H_m) \tag{59a}$$

in the fourth quadrant, in which $H$ and $M(H)$ are replaced by $-H$ and $-M(H)$. Equation (59a) is the same as Eq. (24) for stage II of the initial curve. For the case $a = b$, applicable to cylinders of radius $a$, Eq. (59a) reduces to Kim's solution for $M(H)$ in the fourth quadrant, Eq. (14) in Ref. 5, and to Hulbert's solution, Eq. (10a) in Ref. 11. In the limit $b \to \infty$, for infinite slabs of thickness $2a$, Eq. (59a) reduces to the solution of Fietz *et al.*, Eq. (c) in Table I of Ref. 9.

## E. Hysteresis loops for the medium-$H_m$ case ($H_p < H_m < H_m^*$)

### 1. Current densities and local fields

For the medium-$H_m$ case, the reverse magnetization process is shown in Figs. 5(a)–5(n). The difference between Figs. 5(a)–5(n) and Figs. 4(a)–4(n) is only for stage II. At the end of stage I [Figs. 5(e) and 5(f)], $H = 0$, but $x_1$ is still greater than 0. Therefore, in stage II, when $H < 0$, $J(x)$ has to be divided into three parts: $J_m(x)$, $J_2(x)$, and $J_3(x)$, shown in Figs. 5(g) and 5(h). The next stage starts from the point where $x_2 = 0$, as shown in Figs. 5(i) and 5(j). The expressions for $J(x)$ are the same as in the high-$H_m$ case.

### 2. Stage I ($0 < H < H_m$)

This stage is the same as for the high-$H_m$ case except for the field interval, which is from $H_m$ to 0 here.

### 3. Stage II ($H_{prm} < H < 0$)

In stage II, $H_i(x)$ and $M(x)$ are

$$H_i(x) = H_m + \int_x^a J_m(x)dx \quad (0 < x < x_2)\,, \tag{61a}$$

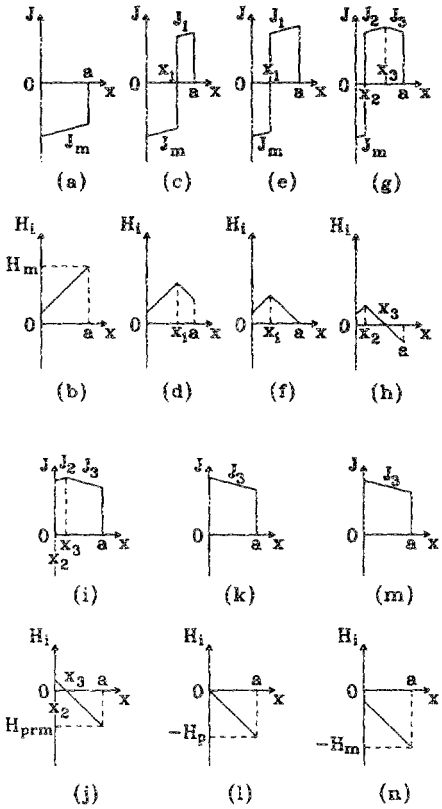


FIG. 5. Same as Fig. 3, from $H_m$ between $H_p$ and $H_m^*$.

$$H_i(x) = H + \int_x^{x_3} J_2(x)dx + \int_{x_3}^a J_3(x)dx \quad (x_2 < x < x_3)\,, \tag{61b}$$

$$H_i(x) = H + \int_x^a J_3(x)dx \quad (x_3 < x < a)\,, \tag{61c}$$

and

$$M_i(x) = H_m - H + \int_x^a J_m(x)dx \quad (0 < x < x_2)\,, \tag{62a}$$

$$M_i(x) = \int_x^{x_3} J_2(x)dx + \int_{x_3}^a J_3(x)dx \quad (x_2 < x < x_3)\,, \tag{62b}$$

$$M_i(x) = \int_x^a J_3(x)dx \quad (x_3 < x < a)\,. \tag{62c}$$

$x_2$ and $x_3$ are given in Eqs. (40b) and (40a), and the final result is

$$M(H) = S_3(a - x_3)(b + x_3)/ab - S_1[x_3^2 + (b - a)x_3]/ab - (S_3^3 - H_0^3)Q_4 - (H_0^3 - R_3^3)Q_5 + (R_3^3 - R_4^3)Q_6 - 2[(a - x_3)H_0^3 + (x_3 - x_2)R_3^3 - x_2R_4^3]/5kab \quad (H_{prm} < H < 0)\,, \tag{63}$$

where $H_{prm}$ is the reverse full-penetration field for the medium-$H_m$ case, which can be determined by taking $x_2 = 0$ in Eq. (40b):

$$H_{prm} = H_0 - [4ka + 2H_0^2 - (H_0 + H_m)^2]^{1/2}. \quad (64)$$

#### 4. Stage III ($-H_p < H < H_{prm}$)

This stage is the same as the high-$H_m$ case except for the interval of $H$, which is here from $H_{prm}$ to $-H_p$.

#### 5. Stage IV ($-H_m < H < -H_p$)

This stage is the same as the high-$H_m$ case.

## IV. COMPUTED $M(H)$ CURVES

We have analytically verified, for each case in Sec. III, that the stages are continuous at their end points. To illustrate the formulas in Sec. III, we give some computed $M(H)$ curves. To reduce the number of variables, we define a new parameter, similar to one used by Kim[5]:

$$p = (2ka)^{1/2}/H_0. \quad (65)$$

Equations (23) and (48) can be rewritten as

$$H_p = H_0[(1+p^2)^{1/2} - 1], \quad (66)$$

$$H_m^* = H_0[(1+2p^2)^{1/2} - 1]. \quad (67)$$

The shapes of the $M(H)$ curves are now determined by $p$ and $b/a$. Figures 6(a)–6(e) give the initial and hysteresis $M(H)$ curves for $b/a = 1$ and $p = 0.3$, 1, 3, 10, and 1000. For each case, five $M(H)$ loops are drawn for $H_m = H_p/2$, $H_p$, $(H_p + H_m^*)/2$, $H_m^*$, and $4H_p$. The curves in Figs. 7(a) and 7(b) give the initial and hysteresis $M(H)$ curves for $p = 1, H_m = H_m^*$ and $4H_p$, and $b/a = 1$ (smallest), 1.5, 2, 5, and 100 (largest). For all the curves, $M$ and $H$ are normalized to $H_p$.

We can observe from Figs. 6(a)–6(e) that the $M(H)$ curves derived from Kim's model have a wide variety. The curves shown in Fig. 6(a) are very similar to those derived from Bean's model.[2] If $p$ were smaller than 0.1, there would be virtually no difference between Kim's and Bean's models. Figure 6(e) for $p = 1000$ is almost the same as for the limiting case $p \to \infty$, where Kim's model reduces to $J_c(H_i) = k/H_i$.

The initial curves have minima except when $p = 0$. We can see from Figs. 6(a)–6(e) that, with increasing $p$, the field where the minimum is located decreases from $H_p$ to $0.56\,H_p$, and the minimum $M$ decreases from $-0.33\,H_p$ to $-0.36\,H_p$. The initial slopes of the initial curves are $-1$. For $p = 1000$, the initial curve is linear within 1% up to $0.09\,H_p$, despite the assumption of zero lower critical field in the derivation. This linear region does not come from a Meissner state, but is simply a reflection of a large $J_c$ at low $H_i$.

The initial reverse slopes at the corners of the hysteresis loops in Figs. 6(a)–6(e) are also $-1$. This is a consequence of shielding by surface supercurrent at the beginning of stage I. Because $J_c$ is lower, this 1% linear region is smaller.

The second and the fourth loops correspond to the two boundaries between the low-, medium-, and high-$H_m$ cases. We can see from Figs. 6(a)–6(e) that, for the medium- and high-$H_m$ cases, the initial and the hysteresis curves merge

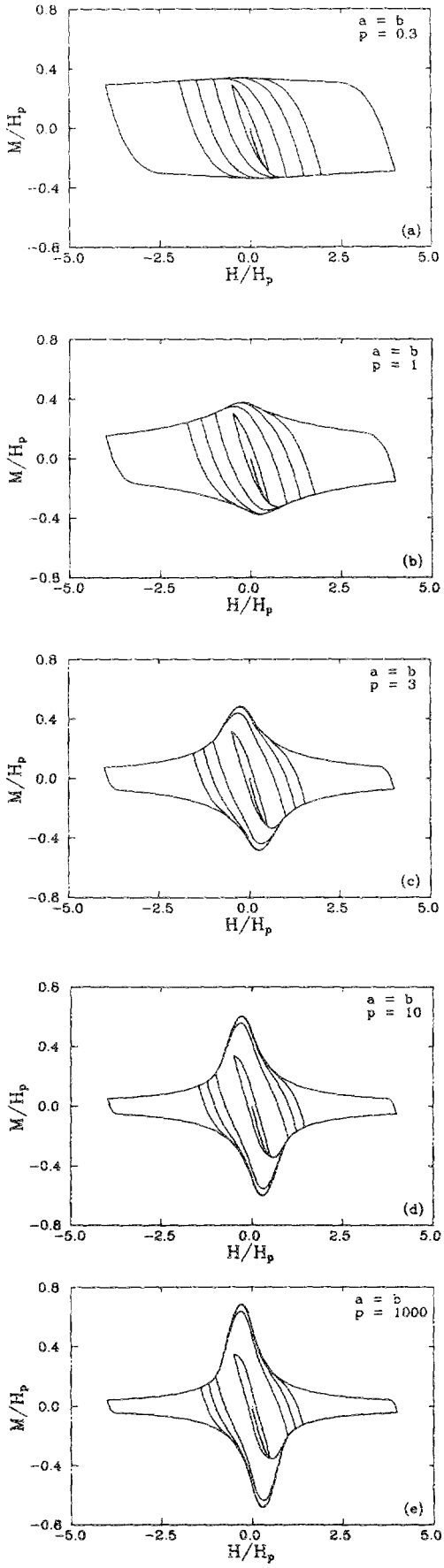


FIG. 6. Theoretical $M$-$H$ curves, scaled by $H_p$, for a sample with $b/a = 1$, for $p =$ (a) 0.3, (b) 1, (c) 3, (d) 10, and (e) 1000. In each figure, loops are shown for $H_m/H_p = 0.5$ (smallest), 1, $\frac{1}{2} + H_m^*/2H_p$, $H_m^*/H_p$, and 4 (largest).

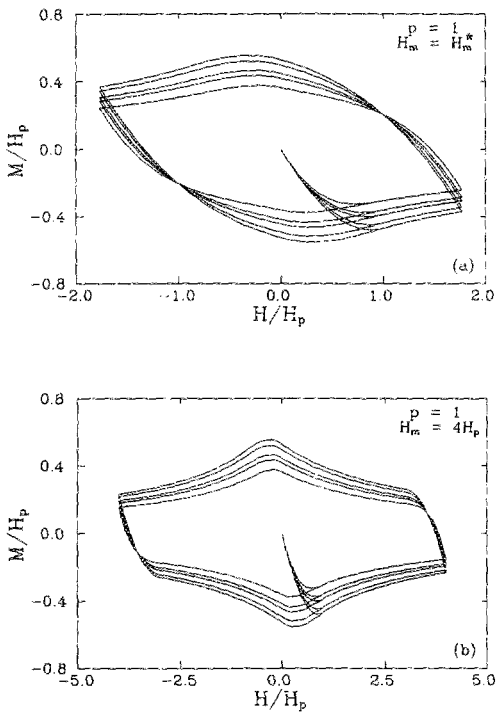


FIG. 7. Theoretical $M$-$H$ curves, scaled by $H_p$, for $p=1$ and (a) $H_m = H_m^*$, (b) $H_m = 4H_p$. In each figure, curves are shown for samples with aspect ratio $b/a = 1$ (smallest), 1.5, 2, 5, and 100 (largest).

when $H \gg H_p$. The middle parts, around $H=0$, are the same for all the loops in the high-$H_m$ case.

With increasing $b/a$, the width of the normalized hysteresis loop increases asymptotically, as seen in Figs. 7(a) and 7(b). One interesting feature in Figs. 7(a) and 7(b) is that, for each figure, the loops with the same $p$ and $H_m$ cross at two points. This crossover effect is general for $H_m > H_p$. For $H_m = H_m^*$ the crossing points are at $H = \pm H_p$, but for higher $H_m$ the points are at higher fields. For a set of samples with the same $a$ and different $b$, when $H = H_m$, $H_i(0)$ should be the same for all the samples, because $H_i$ is a function only of $x$. When $H$ is reduced from this $H_m$ to a value $H_{cro}$ that equals this $H_i(0)$, $x_1$ will become $a/2$. Changing the variable in Eq. (7) such that $\xi = x - a/2$, we have

$$M_{cro} = \frac{1}{ab}\int_{-a/2}^{+a/2} (2\xi + b) M_i(\xi)\, d\xi . \tag{68}$$

Because $M_i(\xi)$ is an even function of $\xi$, Eq. (68) can be written as

$$M_{cro} = \frac{1}{a}\int_{-a/2}^{+a/2} M_i(\xi)\, d\xi , \tag{69}$$

independent of $b$. Since both $H_{cro}$ and $M_{cro}$ are independent of $b$ for constant $a$, the point $(H_{cro}, M_{cro})$ must be a crossing point, as illustrated in Figs. 7(a) and 7(b).

## V. $M(H)$ FORMULAS FOR ORTHOHOMBIC SAMPLES IN THE BEAN LIMIT

Bean derived the $M(H)$ formulas for cylindrical and infinite-slab samples for $J_c$ independent of $H_i$. In this paper, we have obtained the $M(H)$ formulas for the orthorhombic geometry using Kim's model for $J_c$, Eq. (1). In this section, we reduce the orthorhombic Kim formulas to general orthorhombic Bean formulas. Finally, we reduce these to the simple cylinder and slab forms.

### A. Bean's model for orthorhombic samples

Bean's model can be written as

$$J_c(H_i) = J_c , \tag{70}$$

where $J_c$ is constant. To modify Kim's model, Eq. (1), for the Bean limit, let

$$k \to \infty , \tag{71a}$$

$$H_0 \to \infty , \tag{71b}$$

$$k/H_0 = J_c . \tag{71c}$$

All the formulas for Kim's model can be reduced to the corresponding ones for Bean's model. For some cases, namely Eqs. (74), (75b), (77a), and (77b) below, it was necessary to use binomial expansions before taking the limits in Eqs. (71a), (71b), and (71c). For the terms raised to the power 3/2 in Eqs. (24), (45), and (51), expansions has to be carried to third order.

The general expression for the supercurrent density can be obtained from Eq. (12):

$$J(x) = \mathrm{sgn}(J) J_c . \tag{72}$$

For each specific case we have

$$J_0 = J_m = -J_c \tag{73a}$$

and

$$J_1 = J_2 = J_3 = J_c . \tag{73b}$$

We do not have to identify $J_1$, $J_2$, and $J_3$ because we do not need to separate $J(x)$ into several sections, since $J_c$ is constant. For the same reason, for every $M(H)$ curve, only one or two stages have to be considered, and for the reverse curves, only two cases have to be considered.

The full-penetration field can be obtained from Eq. (23) as

$$H_p = J_c a . \tag{74}$$

The initial $M(H)$ curve can be derived from Eqs. (21) and (24) as

$$M(H) = -H + (H^2/2J_c)(1/a + 1/b) - H^3/(3J_c^2 ab) \quad (0 < H < H_p) , \tag{75a}$$

$$M(H) = -J_c a(\tfrac{1}{2} - a/6b) \quad (H_p < H) . \tag{75b}$$

Equations (75a) and (75b) may be found in Ref. 15. The reverse curve for the low-$H_m$ $(0 < H_m < H_p)$ case can be derived from Eq. (36) as

$$M(H) = -H + [(H_m^2 + 2HH_m - H^2)/4J_c](1/a + 1/b) - (3H_m^3 + 3H_m^2 H - 3H_m H^2 + H^3)/(12J_c^2 ab) \quad (-H_m < H < H_m) . \tag{76}$$

The reverse curve for the high-$H_m$ $(H_p < H_m)$ case can be derived from Eqs. (45) and (51) as

$$M(H) = -J_c a(\tfrac{1}{2} - a/6b) + H_m - H - [(H_m - H)^2/4J_c](1/a + 1/b) + (H_m - H)^3/(12J_c^2 ab) \quad (H_m - 2H_p < H < H_m), \tag{77a}$$

$$M(H) = J_c a(\tfrac{1}{2} - a/6b) \quad (-H_m < H < H_m - 2H_p). \tag{77b}$$

### B. Reduction to simple geometries

For the infinite slab, $b/a \to \infty$, the above equations for $M(H)$ become, for the initial curve,

$$M(H) = -H + H^2/2J_c a \quad (0 < H < H_p), \tag{78a}$$

$$M(H) = -J_c a/2 \quad (H_p < H); \tag{78b}$$

for the low-$H_m$ ($H_m < H_p$) curve,

$$M(H) = -H + (H_m^2 + 2HH_m - H^2)/4J_c a \quad (-H_m < H < H_m); \tag{79}$$

and for the high-$H_m$ ($H_p < H_m$) curve,

$$M(H) = -J_c a/2 + H_m - H - (H_m - H)^2/4J_c a \quad (H_m - 2H_p < H < H_m), \tag{80a}$$

$$M(H) = J_c a/2 \quad (-H_m < H < H_m - 2H_p). \tag{80b}$$

For the cylinder, $b/a = 1$, the corresponding equations are, for the initial cruve,

$$M(H) = -H + H^2/J_c a - H^3/3(J_c a)^2 \quad (0 < H < H_p), \tag{81a}$$

$$M(H) = -J_c a/3 \quad (H_p < H); \tag{81b}$$

for the low-$H_m$ ($H_m < H_p$) curve,

$$M(H) = -H + (H_m^2 + 2HH_m - H^2)/2J_c a - (3H_m^3 + 3H_m^2 H - 3H_m H^2 + H^3)/12(J_c a)^2 \quad (-H_m < H < H_m); \tag{82}$$

and for the high-$H_m$ ($H_p < H_m$) curve,

$$M(H) = -J_c a/3 + H_m - H - (H_m - H)^2/2J_c a + (H_m - H)^3/12(J_c a)^2 \quad (H_m - 2H_p < H < H_m), \tag{83a}$$

$$M(H) = J_c a/3 \quad (-H_m < H < H_m - 2H_p). \tag{83b}$$

Equations (78a), (78b), (79), (81a), (81b), and (82) for slabs and cylinders are the same as Eqs. (2), (3), and (5) in Ref. 2. Bean did not treat the high-$H_m$ case, only the initial curves and the low-$H_m$ case.

### C. Hysteresis loss

Although this paper deals with magnetization curves rather than hysteresis loss $W$, it is straightforward to calculate energy loss per unit volume per field cycle for orthorhombic samples in the Bean limit. Generally,

$$W = \mu_0 \oint H\, dM \approx \mu_0 \oint M\, dH. \tag{84a}$$

For the complete low-$H_m$ loop, from Eq. (76),

$$W = 2\mu_0 H_m^3 [J_c(a+b) - H_m]/(3J_c^2 ab). \tag{84b}$$

For the complete high-$H_m$ loop, from Eqs. (77a) and (77b),

$$W = 2\mu_0 J_c a [J_c a(a - 2b) + H_m(3b - a)]/3b. \tag{84c}$$

## VI. DETERMINATION OF $J_c(H)$ FROM THE WIDTH OF THE HYSTERESIS LOOP

In this section we discuss two topics. First, we examine the necessary conditions for using Bean's model to determine $J_c$ from hysteresis loop measurements assuming that $J_c(H_i)$ actually follows Eq. (1). Second, we offer a modification of the conventional cylinder and slab formulas for $J_c$ determination for the general orthorhombic Bean model.

### A. Prerequisites for Bean formulation

The traditional way to determine critical-current density of superconductors from magnetic measurements is based on Bean's model, where $J_c$ is considered constant. To determine $J_c(H)$, a hysteresis loop is obtained, and the width of the hysteresis loop at a given field, $\Delta M(H)$, is measured. Bean's model[2] gives

$$J_c(H) = 3\Delta M(H)/2a \tag{85a}$$

for cylinders of radius $a$, and

$$J_c(H) = \Delta M(H)/a \tag{85b}$$

for slabs of thickness $2a$. Note that a field-dependent $J_c$ is contrary to the assumption used to derive the Bean equations.

There are two requirements for using Eqs. (85a) and (85b) for $J_c$ determination if $J_c(H_i)$ is assumed to actually follow Kim's model. (1) The magnetization on ascending and descending branches of the hysteresis loop at a given $H$ must correspond to fully penetrated states. (2) The maximum deviation of $J_c(H_i)$ in the sample from $J_c(H_i = H)$ must be small. $H$ is the uniform applied field, and $H_i$ is the local internal field. The notation $J_c(H_i = H)$ means $J_c(H_i)$ for $H_i = H$ These conditions will be expressed in terms of recommended values of $H_m$, $H$, and $p$.

#### *1. Fully penetrated states*

For fully penetrated states, shielding currents circulate in only one sense throughout the volume of the specimen for the upper branch of the hysteresis loop and in the opposite sense for the lower branch. The condition of full penetration for both branches of the hysteresis loop is satisfied for the high-$H_m$ case (Sec. III D) when

$$H_m \geqslant H_m^* \tag{86}$$

and

$$H \leqslant H_{prh}. \tag{87}$$

If $H_m = H_m^*$, then $H_{prh} = 0$, and the condition is satisfied only for $H = 0$. To obtain a useful $H$ interval, Eq. (86) is restricted to

$$H_m \gg H_m^*. \tag{86a}$$

As examples, we obtain $J(H)$, using Eq. (85a), from the major hysteresis loops in Figs. 6(a)–6(e) (for which $H_m \gg H_m^*$). The symbols in Figs. 8(a)–8(e) give the $J_c(H)$

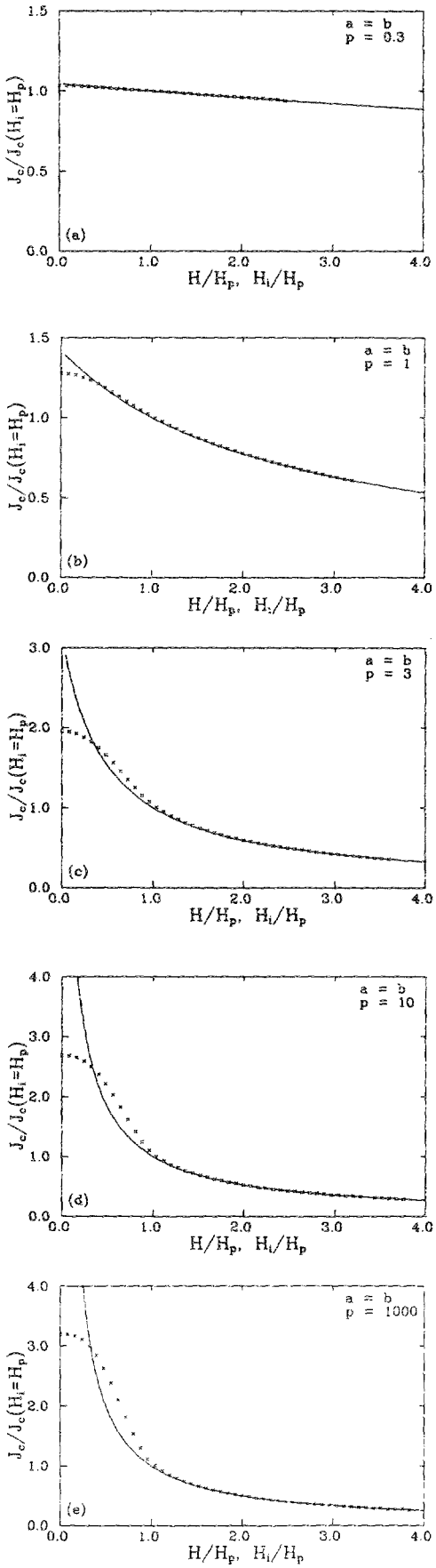


FIG. 8. Comparison of $J_c(H)$ [symbols, obtained from the major loops in Figs. 6(a)–6(e) using Eq. (85a)] with $J_c(H_i)$ [smooth curve, obtained from Eq. (1) which was also used to compute the loops in Fig. 6]. $H$ and $H_i$ are normalized to $H_p$. $J_c(H)$ and $J_c(H_i)$ are normalized to $J_c(H_i = H_p)$.

thus obtained for $p = 0.3$, 1, 3, 10, and 1000. For comparison, the smooth curves in Figs. 8(a)–8(e) give $J_c(H_i)$ derived from Eq. (1). The $H$ scales are normalized to $H_p$, and the $J_c$ scales are normalized to $J_c(H_i = H_p)$. We can see from these figures that $J_c(H)$ and $J_c(H_i)$ overlap in a certain $H$ interval, somewhat different for each case. The upper limit of this correspondence interval is $H_{prh}$, Eq. (47), even for hysteresis loops where $H_m \gg 4H_p$.

### 2. Uniform $J_c(H_i)$

Referring again to Figs. 8(a)–8(e), the lower limit of overlap is about $1.5\,H_p$ for most cases. For the case $p \ll 1$, Fig. 8(a), this limit is much smaller. The reason for the extended overlap range is that $J_c(H_i)$ is rather uniform for small $p$, so that $J_c(H) \simeq J_c(H_i = H)$.

We consider stages II and IV of the hysteresis loop (Sec. III D). From Eqs. (51) and (59a), we obtain $\Delta M(H)$. Dropping the higher-order terms and substituting into Eqs. (85a) and (85b), we obtain

$$J_c(H) = J_c(H_i = H)\{1 + s[\delta H_i(H)]^2\}, \tag{88}$$

where

$$\delta H_i(H) = \Delta H_i(H)/(H_0 + H), \tag{88a}$$

$$\Delta H_i(H) = aJ_c(H_i = H), \tag{88b}$$

and where $s = 1/4$ for $b/a \to \infty$ (infinite slab), and $s = 1/20$ for $b/a = 1$ (cylinder).

The field change relative to $(H_0 + H)$ in the sample is given by Eq. (88a). $\Delta H_i(H)$ defined by Eq. (88b) is the first-order difference between $H_i(0)$ and $H_i(a)$. From Eq. (88), $J_c(H)$ derived from $\Delta M(H)$ is always greater than $J_c(H_i = H)$. The difference between $J_c(H)$ and $J_c(H_i = H)$ is determined by $\delta H_i(H)$, decreasing with decreasing $a$ and $J_c(H_i)$ and increasing $H_0$ and $H$. From the factor $s$, the error in $J_c(H)$ is much smaller for a cylinder than for a slab with the same $a$.

When $H \simeq 0$, we have to consider stages II and III of the loop. The requirements for small errors are the same as for larger $H$ except that $J_c(H)$ is always less than $J_c(H_i = H)$. When $p \ll 1$, $H_0$ is very large, and the error in $J_c(H)$ is very small, even at $H = 0$.

## B. Formula for orthorhombic samples

$\Delta M(H)$ in Eqs. (85a) and (85b) is the vertical width of the hysteresis loop. In Sec. IV, we showed that the vertical width of the hysteresis loop increases with increasing $b/a$. If we use Eq. (85b) to calculate $J(H)$ for the samples with the same $a$ but different $b$, different $J_c$ will be obtained even for the same superconductor material. Thus, we derive a formula for orthorhombic samples using Bean's model. In the penetrated state, using Eq. (18b) with $x_0 = 0$ and $J(x) = -J_c$, we obtain

$$M_i(x) = -J_c(a - x). \tag{89}$$

Substituting Eq. (89) into Eq. (7), or simply subtracting Eqs. (77b) and (75b), we have

$$\Delta M = J_c a(1 - a/3b). \tag{90}$$

Rearranging, we obtain the general formula

$$J_c(H) = \Delta M(H)/[a(1 - a/3b)] . \quad (91)$$

It reduces to Eq. (85a) when $b/a = 1$, and Eq. (85b) when $b/a \to \infty$. Equation (85a) applies to polygons as well as cylinders, following the argument of Sec. II B. Equation (91) has also been derived by Clem.[16]

## VII. CONCLUSION

Since the original work of Bean and London, the critical-state model has been used by many researchers to describe the magnetic response of hard type-II superconductors. The model has provided a simple, intuitive framework in which data could be analyzed, despite the need for approximations when applying the model to samples of finite dimensions. The refinements by Kim *et al.* were an effort to incorporate the field dependence of critical-current density. The results were magnetization curves that more closely resembled experimental data, particularly at low fields. Several other authors have attempted, with some success, to extend the critical-state model for various applications.

In this paper we have developed some useful equations for the analysis of magnetization of type-II superconductors within the construct of the critical-state theory. Using Kim's model for critical-current density, Eq. (1), we have analytically derived magnetization equations for the general case of an infinite superconductor with rectangular cross section. Different equations apply to the various parts of the magnetic hysteresis loop. Section III D gave the equations for the most useful case of large maximum applied field. Examples of the possible variety of magnetization curves were given in the figures. If we take different dimensional limits, the solutions apply to infinite slabs, cylinders, and rods with polygonal cross sections.

The general Kim solution can be reduced to a general Bean model for rectangular cross section by reducing the Kim equation for critical-current density (Sec. V A). In the appropriate dimensional limits, these equations become the well known Bean solutions for slabs and cylinders (Sec. V B). A simple formula was derived to relate the width of a measured hysteresis loop to the critical-current density as a function of applied field, for orthorhombic samples in the Bean limit (Sec. VI B).

## ACKNOWLEDGMENTS

We thank J. Nogués for help with computer programming, W. L. Bahn for drawing Figs. 1–5, and J. S. Muñoz, R. Puzniak, V. Skumryev, and K. V. Rao for helpful discussions. We thank M. A. R. LeBlanc for valuable comments and making us aware of Ref. 11. MACSYMA, a symbolic manipulation program produced by Symbolics, Inc., was used to compare the cylinder and slab limits of our equations with the results in Refs. 5, 9, and 11, and to verify the continuity of the stages in Sec. III. This work was supported by the Swedish Board for Technical Development, STU, and the U.S. Department of Energy, Division of High Energy Physics.

[1] C. P. Bean, Phys. Rev. Lett. **8**, 250 (1962).
[2] C. P. Bean, Rev. Mod. Phys. **36**, 31 (1964).
[3] H. London, Phys. Lett. **6**, 162 (1963).
[4] Y. B. Kim, C. F. Hempstead, and A. R. Strnad, Phys. Rev. Lett. **9**, 306 (1962).
[5] Y. B. Kim, C. F. Hempstead, and A. R. Strnad, Phys. Rev. **129**, 528 (1963).
[6] J. H. P. Watson, J. Appl. Phys. **39**, 3406 (1968).
[7] F. Irie and K. Yamafuji, J. Phys. Soc. Jpn. **23**, 255 (1967).
[8] I. M. Green and P. Hlawiczka, Proc. IEE **114**, 1329 (1967).
[9] W. A. Fietz, M. R. Beasley, J. Silcox, and W. W. Webb, Phys. Rev. **136**, A335 (1964).
[10] V. R. Karasik, N. G. Vasil'ev, and V. G. Ershov, Sov. Phys. JETP **32**, 433 (1971) [Zh. Eksp. Teor. Fiz. **59**, 790 (1970)].
[11] J. A. Hulbert, Brit. J. Appl. Phys. **16**, 1657 (1965).
[12] M. C. Ohmer and J. P. Heinrich, J. Appl. Phys. **44**, 1804 (1973).
[13] J. J. Wollan and M. C. Ohmer, Cryogenics **16**, 271 (1976).
[14] G. Ravi Kumar and P. Chaddah, Phys. Rev. B **39**, 4704 (1989).
[15] A. M. Campbell and J. E. Evetts, Adv. Phys. **21**, 199 (1972).
[16] J. R. Clem, cited in: A. Umezawa, G. W. Crabtree, J. Z. Liu, H. W. Weber, W. K. Kwok, L. H. Nunez, T. J. Moran, C. H. Sowers, and H. Claus, Phys. Rev. B **36**, 7151 (1987).